Supplementary Material

Augusto Getirana*[1,2], Hiroko Kato Beaudoing[1,3], Sujay Kumar[1], Matthew Rodell[1]

[1]Hydrological Sciences Laboratory, NASA Goddard Space Flight Center, Greenbelt, MD, United States

[2] Science Systems and Applications, Inc., Lanham, Maryland, USA

[3]Earth System Science Interdisciplinary Center, University of Maryland, College Park, MD

*Corresponding author (augusto.getirana@nasa.gov)

Supplementary Text

Supplementary Text S1. GLDAS-2 land surface model description

GLDAS-2 uses Noah[1] version 3.6, which includes four soil layers (layer depths are 0-10, 10-40, 40-100, and 100-200 cm), a single-layer snowpack, and frozen-soil physics. Infiltration and surface runoff generation in Noah are controlled by the Simple Water Balance (SWB) parameterization[2]. SWB derives surface runoff by statistically averaging a point infiltration-excess formulation to represent nonlinear soil-moisture and infiltration behavior during storm and inter-storm periods. Subsurface runoff is represented as free drainage from the soil column, without capillary rise or interaction with a dynamic aquifer below the 2-m soil column; thus, Noah does not include a separate groundwater storage reservoir in this configuration.

Noah Multi-parameterization version 4.0.1 (Noah-MP) uses the same four-layer, 2-m soil column as Noah and a multilayer snow scheme with up to three snow layers. In this study, Noah-MP was configured with the TOPMODEL-based SIMGM runoff and groundwater scheme[3], which includes a dynamic unconfined aquifer below the soil column. The Ball-Berry stomatal resistance option and climatological vegetation (i.e., dynamic vegetation off) were used; other model options followed the standard configuration.

VIC version 4.1.2 includes a three-layer soil column, a two-layer snowpack[4], frozen-soil physics[5], and nonlinear baseflow[6]. Spatial variability in soil-water storage capacity is represented by the variable infiltration curve. Surface runoff is generated over portions of the grid cell where precipitation added to soil-water storage exceeds the local storage capacity, following the Xinanjiang-type formulation[7,8]. Subsurface baseflow is generated from the lowest soil layer using the nonlinear Arno/Nijssen formulation[6,9]. VIC does not include a separately diagnosed groundwater storage reservoir in this configuration.

CLSM Fortuna 2.5 differs fundamentally from the vertically layered LSMs. Rather than discretizing the subsurface into fixed soil layers, CLSM represents catchment-scale moisture relative to equilibrium conditions using three prognostic states: surface excess, root-zone excess, and catchment deficit[10]. These states determine the fractional areas of hydrological regimes, including saturated, unsaturated but transpiring, and below-wilting-point conditions, with runoff and evaporation varying among regimes. Its TOPMODEL-based formulation[11] uses topographic statistics to represent sub-grid variations in saturation and infer water-table behavior. Precipitation falling on the saturated fraction becomes overland runoff, whereas infiltration in unsaturated

fractions varies with sub-catchment heterogeneity. Groundwater/subsurface storage is diagnosed from the catchment storage formulation rather than represented as a prognostic aquifer comparable to Noah-MP. CLSM also includes a three-layer snow model[12].

Supplementary Text S2. Surface water storage effect on regional terrestrial water storage trends

SWS improves trend agreement in California, Texas, Itaipu, Eastern Brazil, and the Tigris–Euphrates, whereas it degrades agreement in the Central Amazon, Aswan, and Northern India (Supplementary Fig. S3 and Table S1). In most regions, the SWS contribution is small relative to the remaining model–GRACE trend discrepancy. In Northern India, for example, GRACE declines by −32.6 $mm \cdot yr^{-1}$, whereas SWS trends are positive in all four simulations (0.42 to 0.71 $mm \cdot yr^{-1}$), further increasing the discrepancy. In the Tigris–Euphrates, SWS trends are negative in all simulations (−0.35 to −0.87 $mm \cdot yr^{-1}$) and therefore improve trend agreement, but remain small relative to the −21.0 $mm \cdot yr^{-1}$ GRACE trend. Two notable exceptions are the Central Amazon and Itaipu, where SWS substantially modifies the modeled trend: negative SWS trends of −6.1 to −8.8 $mm \cdot yr^{-1}$ strongly degrade agreement with the 20.4 $mm \cdot yr^{-1}$ GRACE trend in the Central Amazon, whereas positive SWS trends of 1.7 to 2.9 $mm \cdot yr^{-1}$ bring modeled TWS trends close to the 5.8 $mm \cdot yr^{-1}$ GRACE trend near Itaipu. Thus, the ability of Noah and VIC to represent aggregate TWS variability after SWS is included does not result from systematic transfer of an omitted groundwater trend into routed surface water. Note that many trend values are not statistically significant (see Supplementary Table S1).

Supplementary Figures

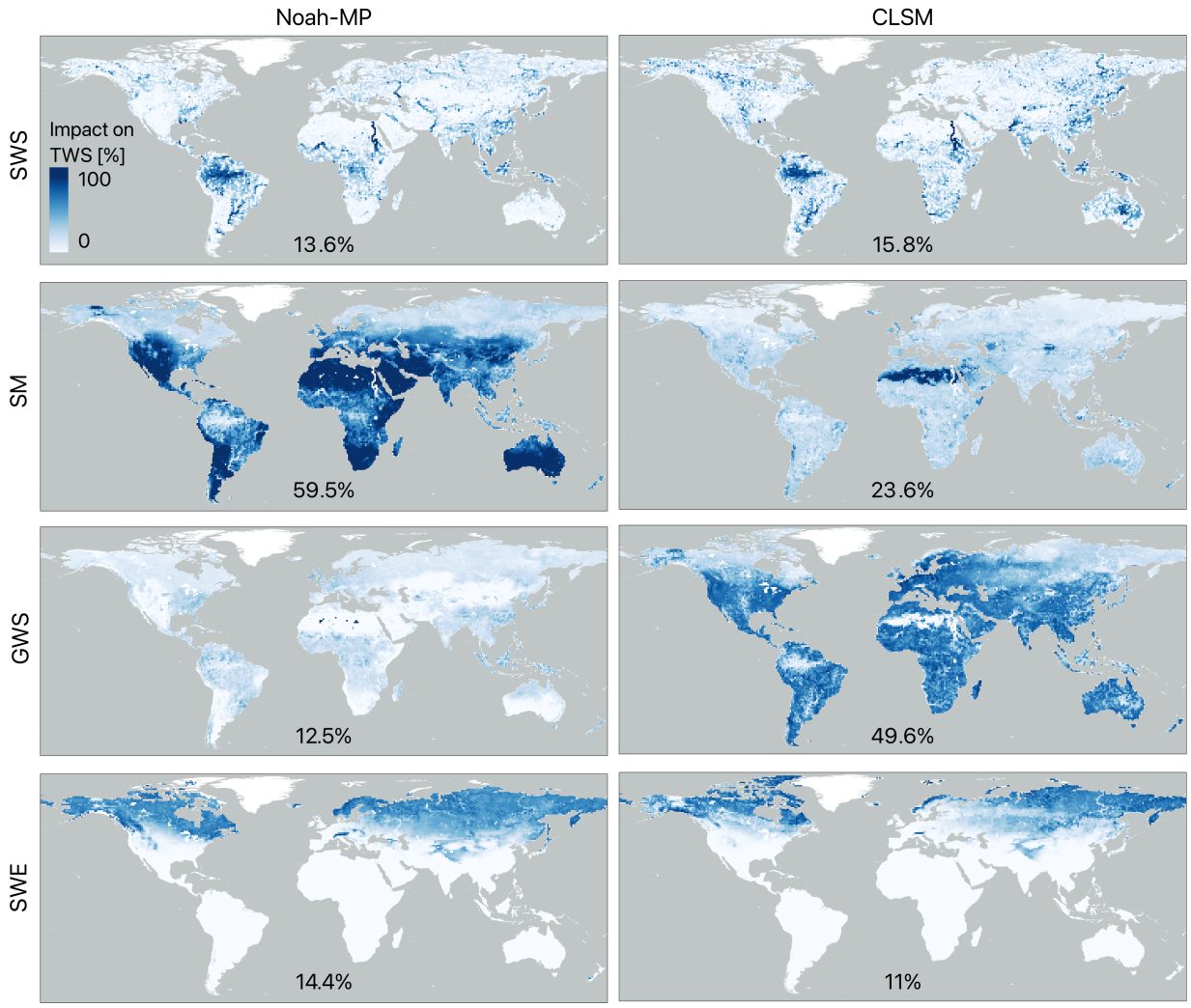

Supplementary Figure S1. Relative contributions of terrestrial water storage components in Noah-MP and CLSM. Spatial distributions of impact indices of individual storage components on modeled terrestrial water storage (TWS) variability for Noah-MP (left) and CLSM (right). Rows show, from top to bottom, surface water storage (SWS), soil moisture (SM), groundwater storage (GWS), and snow water equivalent (SWE). Impact indices are expressed as percentages and sum to 100% at each grid cell.

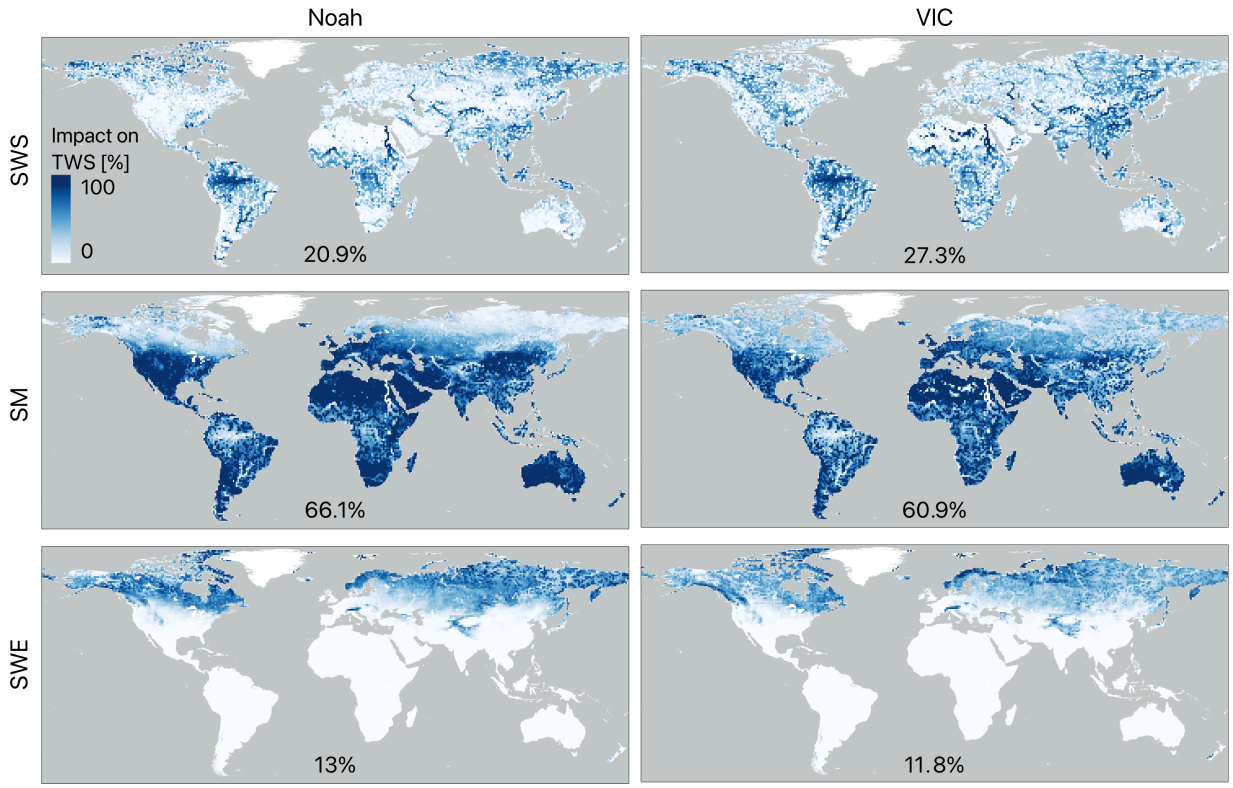

Supplementary Figure S2. Relative contributions of terrestrial water storage components in Noah and VIC. Spatial distributions of impact indices of individual storage components on modeled terrestrial water storage (TWS) variability for Noah (left) and VIC (right). Rows show, from top to bottom, surface water storage (SWS), soil moisture (SM), and snow water equivalent (SWE). Impact indices are expressed as percentages and sum to 100% at each grid cell. Neither Noah nor VIC includes a separately diagnosed groundwater storage component.

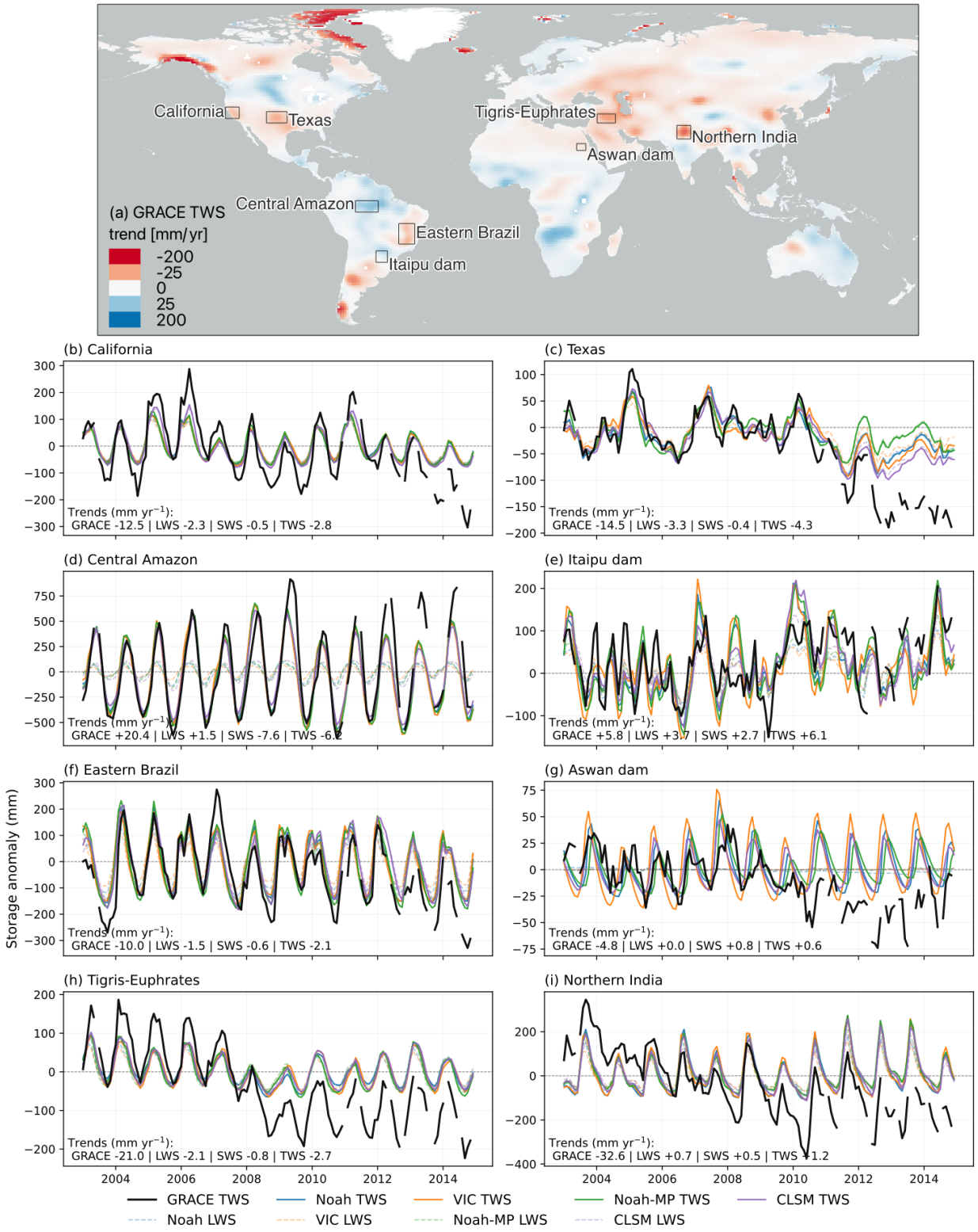

Supplementary Figure S3. Regional terrestrial water storage (TWS) variability and 2003–2014 linear trends. (a) GRACE TWS linear trends over 2003–2014, with boxes indicating the eight regions selected for regional analysis. Panels (b–i) show area-averaged monthly GRACE

TWS anomalies and modeled land water storage (LWS) and TWS anomalies from the four GLDAS-2 land surface models coupled with HyMAP-3: Noah, VIC, Noah-MP, and CLSM. The regions are (b) California, (c) Texas, (d) Central Amazon, (e) Itaipu dam, (f) Eastern Brazil, (g) Aswan dam, (h) Tigris–Euphrates, and (i) Northern India. Modeled TWS is defined as LWS plus the corresponding model-consistent HyMAP-3 surface water storage (SWS). Linear trends reported for each region were calculated over the 2003–2014 study period and are expressed in $mm \cdot yr^{-1}$.

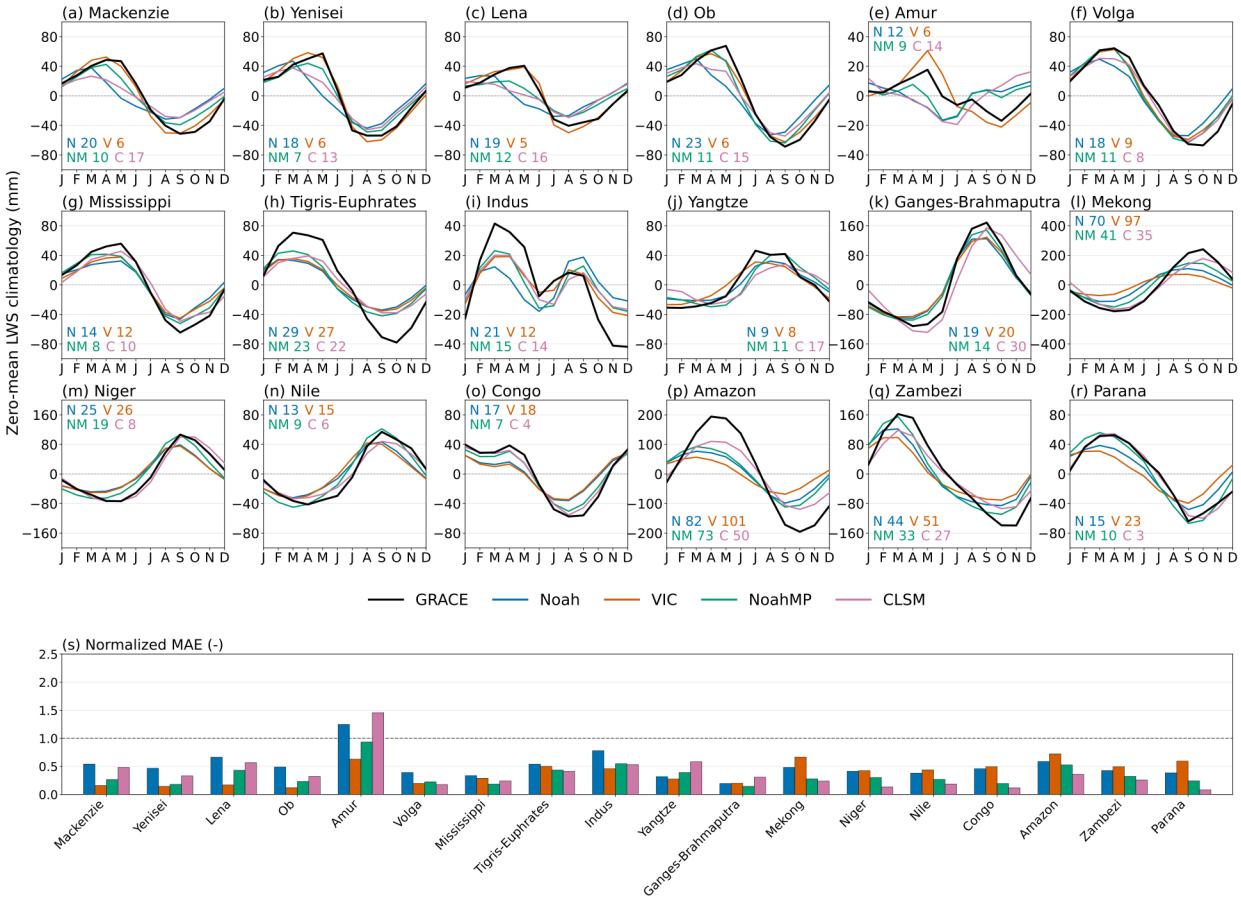

Supplementary Figure S4. Basin-scale seasonal cycles of modeled land water storage and GRACE terrestrial water storage anomalies. Panels (a–r) show zero-mean monthly terrestrial water storage (TWS) climatologies for 18 major river basins from GRACE and land water storage (LWS) climatologies from four GLDAS-2 LSMs. Modeled LWS excludes HyMAP-3 surface water storage. For each basin, calendar-month means were calculated using the same valid monthly samples across GRACE and all four models, and the annual mean of each climatology was removed to isolate the seasonal cycle. Numbers within each panel report the mean absolute error (MAE; mm) of each modeled climatology relative to GRACE. Panel (s) summarizes normalized MAE for each model and basin, calculated as the climatology MAE divided by the standard deviation of the zero-mean GRACE monthly climatology. The dashed horizontal line in panel (s) marks a normalized MAE of one.

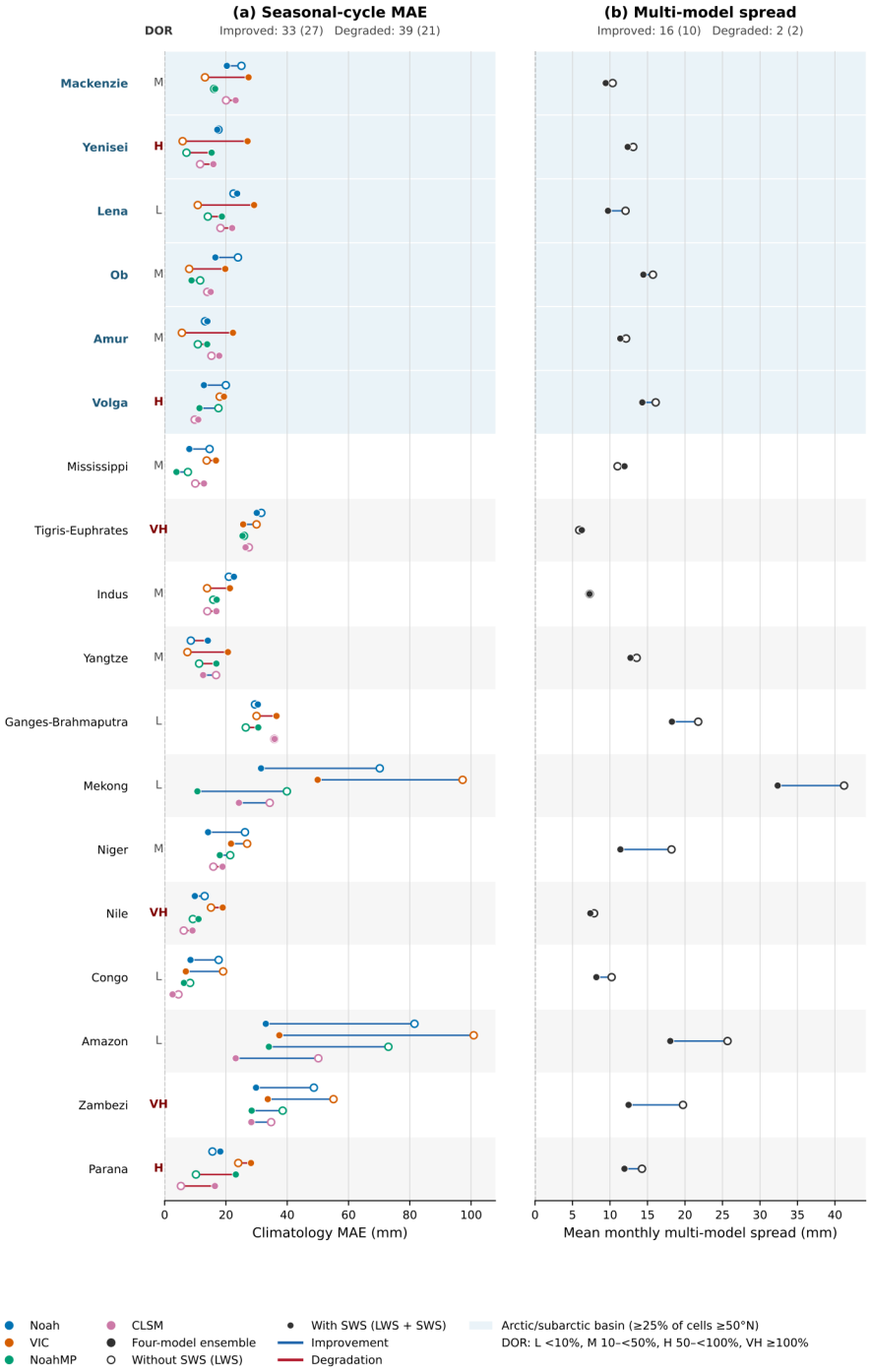

Supplementary Figure S5. Basin-scale effects of surface water storage on seasonal TWS errors and multi-model spread. Paired diagnostics are shown for the 18 major river basins evaluated in the main text. (a) Mean absolute error (MAE) of the modeled monthly TWS climatology relative to GRACE and (b) multi-model spread-to-signal ratio among the four GLDAS-2 land surface models. Open and filled symbols represent simulations without and with HyMAP-3 surface water storage (SWS), respectively, and connecting lines indicate the change

produced by adding SWS. Lower values indicate improved agreement with GRACE in panel (a) and greater convergence among models in panel (b).

Supplementary Tables

Supplementary Table S1. Regional linear trends in terrestrial and surface water storage from GRACE and the four land surface models. Linear trend estimates were obtained for each region defined in Supplementary Fig. S3 from monthly seasonality-removed storage time series. GRACE values represent observed terrestrial water storage (TWS), whereas modeled values are reported separately for land water storage (LWS), surface water storage (SWS), and total modeled TWS (LWS + SWS). Values represent fitted rates of change over the analysis period and are expressed in $mm \cdot yr^{-1}$. Stars (*) indicate statistically significant trends ($q<0.05$).

Region	Simulation	GRACE TWS trend	LWS trend	SWS trend	TWS trend
California	Noah	-12.5*	-2.4	-0.5*	-2.9
	VIC		-2	-0.6	-2.5
	Noah-MP		-2.2	-0.4*	-2.6
	CLSM		-3.8*	-0.3	-4.1*
Texas	Noah	-14.5*	-3.7	-0.3	-4
	VIC		-3.0*	-1.7*	-4.7*
	Noah-MP		-1.4	-0.1	-1.5
	CLSM		-5.5	-0.6*	-6.1
Central Amazon	Noah	20.4*	1.5	-7.6	-6.2
	VIC		0.9	-8.8	-7.9
	Noah-MP		1.5	-7.7	-6.1
	CLSM		2.1	-6.1	-4
Itaipu dam	Noah	5.8	3.3*	2.9*	6.3*
	VIC		2.8	2.8	5.6
	Noah-MP		4.0*	2.6	6.6*
	CLSM		4.1	1.7	5.8
Eastern Brazil	Noah	-10	-1.5	-0.6	-2.2
	VIC		-1.4	-0.5	-2
	Noah-MP		-2.2	-0.8	-3.1
	CLSM		-1.3	-0.1	-1.4
Aswan dam	Noah	-4.8*	-0.4*	0.9	0.4
	VIC		0.0*	0.8*	0.9*
	Noah-MP		0.1*	0.7*	0.8*
	CLSM		0	0.3	0.4
Tigris-Euphrates	Noah	-21*	-2.1	-0.8	-2.9
	VIC		-1.8	-0.7	-2.6*
	Noah-MP		-2.5*	-0.9	-3.4*
	CLSM		-2.2*	-0.3	-2.5*

Northern India	Noah	-32.6*	0.5	0.4	0.9
	VIC		1	0.5	1.5
	Noah-MP		1.9	0.7	2.6
	CLSM		0.4	0.5	0.9

123
124

Supplementary References

1. Ek, M. B. *et al.* Implementation of Noah land surface model advances in the National Centers for Environmental Prediction operational mesoscale Eta model. *Journal of Geophysical Research: Atmospheres* **108**, (2003).
2. Chen, F. *et al.* Modeling of land surface evaporation by four schemes and comparison with FIFE observations. *Journal of Geophysical Research: Atmospheres* **101**, 7251–7268 (1996).
3. Niu, G.-Y., Yang, Z.-L., Dickinson, R. E., Gulden, L. E. & Su, H. Development of a simple groundwater model for use in climate models and evaluation with Gravity Recovery and Climate Experiment data. *Journal of Geophysical Research* **112**, D07103 (2007).
4. Andreadis, K. M., Storck, P. & Lettenmaier, D. P. Modeling snow accumulation and ablation processes in forested environments. *Water Resources Research* **45**, (2009).
5. Cherkauer, K. A. & Lettenmaier, D. P. Hydrologic effects of frozen soils in the upper Mississippi River basin. https://agupubs.onlinelibrary.wiley.com/doi/epdf/10.1029/1999JD900337 (1999) doi:10.1029/1999JD900337.
6. Nijssen, B., O'Donnell, G. M., Lettenmaier, D. P., Lohmann, D. & Wood, E. F. Predicting the Discharge of Global Rivers. https://journals.ametsoc.org/view/journals/clim/14/15/1520-0442_2001_014_3307_ptdogr_2.0.co_2.xml (2001).
7. Wood, E. F., Lettenmaier, D. P. & Zartarian, V. G. A land-surface hydrology parameterization with subgrid variability for general circulation models. *Journal of Geophysical Research: Atmospheres* **97**, 2717–2728 (1992).
8. Ren-Jun, Z. The Xinanjiang model applied in China. *Journal of Hydrology* **135**, 371–381 (1992).

9. Todini, E. The ARNO rainfall—runoff model. *Journal of Hydrology* **175**, 339–382 (1996).
10. Koster, R. D., Suarez, M. J., Ducharne, A., Stieglitz, M. & Kumar, P. A catchment-based approach to modeling land surface processes in a general circulation model: 1. Model structure. *Journal of Geophysical Research: Atmospheres* **105**, 24809–24822 (2000).
11. Beven, K. J. & Kirkby, M. J. A physically based, variable contributing area model of basin hydrology. *Hydrological Sciences Bulletin* **24**, 43–69 (1979).
12. Stieglitz, M., Ducharne, A., Koster, R. & Suarez, M. The Impact of Detailed Snow Physics on the Simulation of Snow Cover and Subsurface Thermodynamics at Continental Scales. https://journals.ametsoc.org/view/journals/hydr/2/3/1525-7541_2001_002_0228_tiodsp_2_0_co_2.xml (2001).